Development of broad modulus profile upon polymer-polymer interface formation between immiscible glassy-rubbery domains

Yannic J. Gagnon, Justin C. Burton, and Connie B. Roth*
Department of Physics, Emory University, Atlanta, Georgia 30322 USA

*Author to whom correspondence should be addressed: cbroth@emory.edu

Published in the *Proceedings of the National Academy of Sciences* on December 26, 2023,
submitted July 21, 2023, revised version accepted November 1, 2023

Abstract: Interfaces of glassy materials such as thin films, blends, and composites create strong unidirectional gradients to the local heterogeneous dynamics that can be used to elucidate the length scales and mechanisms associated with the dynamic heterogeneity of glasses. We focus on bilayer films of two different polymers with very different glass transition temperatures (T_g) where previous work has demonstrated a long-range (∼200 nm) profile in local $T_g(z)$ is established between immiscible glassy and rubbery polymer domains when the polymer-polymer interface is formed to equilibrium. Here, we demonstrate that an equally long-ranged gradient in local modulus $\widetilde{G}(z)$ is established when the polymer-polymer interface (≈5 nm) is formed between domains of glassy polystyrene (PS) and rubbery poly(butadiene) (PB), consistent with previous reports of a broad $T_g(z)$ profile in this system. A continuum physics model for the shear wave propagation caused by a quartz crystal microbalance (QCM) across a PB/PS bilayer film is used to measure the viscoelastic properties of the bilayer during the evolution of the PB/PS interface showing the development of a broad gradient in local modulus $\widetilde{G}(z)$ spanning ≈180 nm between the glassy and rubbery domains of PS and PB. We suggest these broad profiles in $T_g(z)$ and $\widetilde{G}(z)$ arise from a coupling of the spectrum of vibrational modes across the polymer-polymer interface as a result of acoustic impedance matching of sound waves with $\lambda \sim 5$ nm during interface broadening that can then trigger density fluctuations in the neighboring domain.

Significance: How variations in density fluctuations across glasses influence local heterogeneous dynamics is central to understanding amorphous materials and the glass transition. Placing glassy and rubbery polymer domains in contact, we experimentally demonstrate the emergence of a long-range ∼200 nm gradient in local modulus as the polymer-polymer interface forms, in agreement with previously reported long-range ∼200 nm gradients in local glass transition temperature. We propose vibrational waves ∼5 nm that interact with localized soft collective excitations propagate across the ∼5 nm polymer-polymer interface when formed coupling the vibrational spectrum and causing density fluctuations that influence collective α-relaxation events and associated local properties over long distances. These observations make visible a long-range mechanism not included in current theoretical efforts.

Keywords: glasses | interfacial perturbations | polymer-polymer interfaces | modulus | quartz crystal microbalance

Glasses are characterized by spatial and dynamical heterogeneities in their local mobility associated with local packing frustrations. One method of accessing information about the nature of these heterogeneous dynamics and their length scales is to study systems with a perturbing interface that creates a strong unidirectional gradient to the local mobility (1–6). Several years ago Baglay and Roth used localized pyrene fluorescence to map the profile in local glass transition temperature $T_g(z)$ as a function of position across a polymer-polymer interface between two semi-infinite domains of poly(n-butyl methacrylate) (PnBMA) and polystyrene (PS), two immiscible polymers whose difference in bulk T_g spanned $\Delta T_g = T_{g\ \mathrm{PS}}^{\mathrm{bulk}} - T_{g\ \mathrm{PnBMA}}^{\mathrm{bulk}} = 80$ K (7). This weakly immiscible system showed a remarkably broad and asymmetric $T_g(z)$ profile (Fig. 1A) that was well fit by a sigmoidal curve of the form $T_g(z) = T_g^{\mathrm{av}} + \frac{1}{2}\Delta T_g \tanh\left[\frac{2(z-\gamma)}{W_{T_g}}\right]$, where the width of this broad $T_g(z)$ profile $W_{T_g} = 230$ nm and offset $\gamma = 80$ nm was biased towards the stiffer glassier polymer. Similar broad $T_g(z)$ profiles have since been measured in a number of other weakly immiscible polymer systems all with compositional interfacial widths $w_I = 5$–7 nm, including PS and poly(butadiene) (PB) (Fig. 1A) (8, 9).

One of the key findings from these results was that this broad $T_g(z)$ profile does not occur unless the interface between the two dissimilar polymers is annealed to equilibrium (4, 8). The interface that forms between two immiscible polymers upon annealing at elevated temperature above the T_g^{bulk} of both polymers reflects a competition between the entropic penalty of distorting the chain at a sharp interface and the energetic cost of creating more unfavorable monomer-monomer contacts. This balance results in an equilibrium composi-

tion profile $\phi(z) = \frac{1}{2}\left[1 + \tanh\left(\frac{2z}{w_I}\right)\right]$ with an interfacial width $w_I = \frac{2b}{\sqrt{6\chi}}$ for high molecular weight polymers that strongly depends on the interaction parameter χ between the polymer pair, where b is the statistical segment length of order a monomer size (10). The broad $T_g(z)$ profiles were observed for weakly immiscible systems with w_I = 5–7 nm (7–9), while recent work by Gagnon and Roth on the much more strongly immiscible PS/PDMS system with $w_I \approx 1.5$ nm found the breadth of the $T_g(z)$ profile to be reduced by a factor of three (11). A second key finding was the demonstration by Gagnon and Roth that the magnitude of the local $T_g(z)$ in PS at a distance of $z = 50$ nm from a PS/PDMS interface shifted by 40 K simply by varying the rubbery polydimethylsiloxane (PDMS) modulus between $E = 0.9$–2.6 MPa (11). From these observations, we conclude that the width of the interface and the difference in modulus between the two domains are key factors in understanding the emergence of these broad ∼200 nm long-range dynamical gradients in local T_g.

These long-ranged ∼200 nm $T_g(z)$ perturbations observed across polymer-polymer interfaces are in strong contrast to the much shorter ranged ∼20 nm gradients observed next to free surfaces (polymer-air), polymer-substrate, or even polymer-liquid interfaces (2, 4, 12). Recent theoretical efforts have made good progress in understanding these shorter ranged ∼10 nm gradients, but have called for new insight needed to understand the ∼100 nm longer-ranged gradients observed with polymer-polymer interfaces (3). Noting that these shorter ranged ∼10 nm gradient systems have sharp interfaces with widths of only ∼0.5 nm, we believe that these differences in dynamical gradients arise from how vibrational waves are able to propagate across the sample, where broad polymer-polymer interfaces allow for a coupling of the vibrational density of states (VDoS), particularly around the boson peak, between polymer domains via acoustic impedance matching. Even though computer simulations have observed T_g shifts within polymer domains that depend on the interaction parameter χ (proportional to interfacial width) and difference in Debye-Waller factors (proportional to modulus) between polymer domains, the observed lengthscales of the dynamical gradient are still modest (13, 14). However, we note studies have shown that common computational practices of truncating Lennard-Jones potentials and use of finite system sizes with periodic boundary conditions limit the strength of interactions and alter the VDoS, particularly the strength and position of the boson peak (15, 16).

The VDoS in glasses has long been recognized as being anomalous relative to crystalline materials with an excess of vibrational modes above the Debye prediction referred to as the boson peak (17–19). Low-energy quasilocalized excitations (QLEs) associated with collective oscillations near soft potential regions are found to emerge

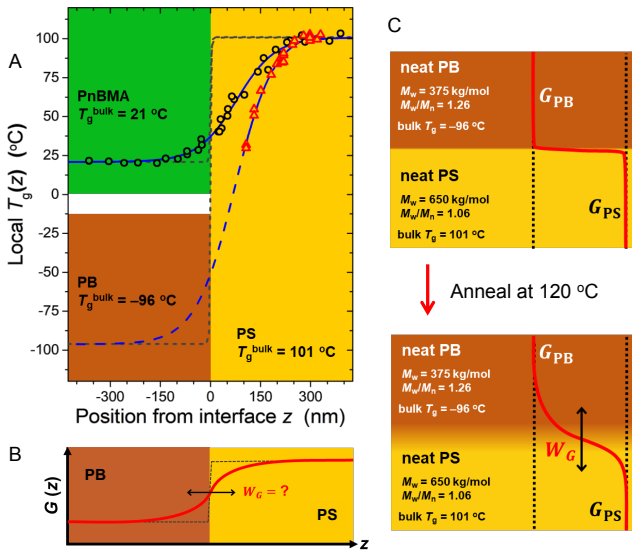

Fig. 1: (A) Local glass transition temperature $T_g(z)$ profile measured with local pyrene fluorescence for semi-infinite bilayers of PnBMA/PS (black circles) and PB/PS (red triangles) annealed to equilibrium [Data taken from Refs. 7–9]. Blue curves are hyperbolic tangent fits to the $T_g(z)$ data with widths of W_{T_g} = 230 nm (7–9), while the gray dashed curves are the composition profiles $\phi(z)$ with interfacial widths w_I = 5–7 nm. (B) Is a correspondingly broad gradient in local modulus $\widetilde{G}(z)$ with width W_G also developing upon polymer-polymer interface formation? (C) Cartoon geometry of PB/PS bilayers investigated in this study, initially with only minimal annealing at 25 °C for 20 h ($w_I \approx 1$ nm) and after annealing at 120 °C for a time t_a up to 100 min leading to $w_I \approx 5$ nm.

upon vitrification (20, 21), which have been computationally linked to locations of cooperative α-relaxation events at so-called "soft spots" (22–24). These QLEs, of order ∼1 meV (∼1.5 ps^{-1}) in PS (21), will hybridize with propagating sound waves of comparable energy (20, 25, 26), corresponding to frequencies ∼300 GHz and wavelengths $\lambda \sim 5$ nm. We envision that these acoustic waves provide a long-range mechanism by which density fluctuations and α-relaxations can be triggered elsewhere in the system.

The vibrational spectrum in glassy materials strongly depends on the overall boundary conditions of the system. For these $\lambda \sim 5$ nm sound waves, sharp interfaces (∼0.5 nm) will cause reflections, as has already been demonstrated by computer simulations and inelastic neutron scattering experiments showing changes in the VDoS associated with different kinds of confinement (27–32). In contrast, the broader interfacial widths of polymer-polymer interfaces ($w_I \approx 5$ nm) will appear nearly continuous to these $\lambda \sim 5$ nm sound waves, allowing these acoustic phonons to propagate across the interface if the difference in acoustic impedance $\widetilde{Z} = \sqrt{\rho \widetilde{G}}$ is not too large between the two polymer domains, where $\widetilde{G}(\omega) = G'(\omega) + i\,G''(\omega)$ is the complex shear modu-

lus and ρ the density (33, 34). We think it is this transmission of vibrational waves of $\lambda \sim 5$ nm associated with the glass transition that can occur across the polymer-polymer interface when the interface is annealed to equilibrium ($w_I \approx 5$ nm) that enables coupling of local glass transition dynamics across the interface causing the broad $T_g(z)$ profiles observed. The question then becomes, does the emergence of this broad profile in local $T_g(z)$ also result in broad profiles of other local property changes across the polymer-polymer interface such as modulus?

In the present work, we experimentally test for the emergence of a gradient in modulus $\widetilde{G}(z)$ upon annealing of a glassy-rubbery PS/PB bilayer film. An important open question associated with understanding local T_g changes near interfaces is determining the degree to which other local material properties, typically correlated with T_g in the bulk, are also altered locally in these systems (4, 35). In bulk, the modulus of a polymer changes by three orders of magnitude on vitrification through the glass transition (36). As such, the development of a broad profile in local $T_g(z)$ upon polymer-polymer interface formation would be expected to be associated with the development of a broad profile in local modulus $\widetilde{G}(z)$, as illustrated in Fig. 1B. Using a quartz crystal microbalance (QCM) as a high-frequency rheometer (37), we observe the decreased dissipation associated with the increased transmission of QCM shear waves across the PS/PB interface upon polymer-polymer interface formation as the PS/PB interface is progressively annealed at elevated temperature. Analyzing the QCM frequency $\Delta f(n)$ and dissipation $\Delta\Gamma(n)$ shifts as a function of harmonic number n using a multilayer continuum physics model (37), we demonstrate the emergence of a broad modulus profile $\widetilde{G}(z) \approx 180$ nm upon formation of the PB/PS interface that is consistent with the broad $T_g(z)$ profile previously measured in this system (9). These findings lend support to the notion that propagation of acoustic waves across broadened polymer-polymer interfaces leads to strong coupling of local material properties between polymer domains.

Results and Discussion

Bilayer films were made by placing ≈400 nm thick PB layers ($T_g^{\text{bulk}} = -96$ °C, $M_w = 375$ kg/mol) atop ≈1100 nm thick PS layers ($T_g^{\text{bulk}} = 101$ °C, $M_w = 650$ kg/mol) supported on QCM crystals. We are interested in studying the evolution of the frequency $\Delta f(n)$ and dissipation shifts $\Delta\Gamma(n)$ of the QCM as the PB/PS polymer-polymer interface is formed between the layers. The QCM sensor undergoes a shear wave oscillation in the MHz regime, where at its most basic level, the added mass of the sample acts to shift the resonance frequency $\Delta f_n = f_n^{\text{film+QCM}} - f_n^{\text{bare QCM}}$ from the bare crystal response, which can be used as an extremely accurate mass sensor using the well-known Sauerbrey equation (38, 39). However, for viscoelastic samples, there is also a shift in the dissipation $\Delta\Gamma$ (width) of the resonance (39, 40). These shifts in $\Delta f(n)$ and $\Delta\Gamma(n)$, especially at higher harmonic numbers n ($f_n = nf_0$, where f_0 is the fundamental frequency of the bare crystal), can be used to measure the frequency dependent modulus $\widetilde{G}(\omega) = G'(\omega) + iG''(\omega)$ ($\omega = 2\pi f_n$) of the sample. We recently published a study presenting a continuum physics model of the shear wave propagation from the QCM in a rubbery viscoelastic polymer film that allowed us to numerically fit the measured frequency $\Delta f(n)$ and dissipation $\Delta\Gamma(n)$ shifts across a wide range of harmonics n (37). From the nonlinear fits to these data, we were able to measure the frequency dependent complex shear modulus $\widetilde{G}(\omega)$ for rubbery polymer films of PB and PDMS, where the QCM determined frequency dependent storage $G'(\omega)$ and loss $G''(\omega)$ moduli showed good agreement with time-temperature shifted rheometry data from the literature. We expand this continuum physics model here to the study of multilayer films.

As illustrated in Fig. 1C, we will start with PB/PS bilayer samples that are initially only held at 25 °C for 20 h, well below the T_g^{bulk} of PS. As described in the Supplementary Information, initially these bilayer samples after only being held at 25 °C are expected to have a PB/PS interfacial width that is not more than $w_I \approx 1$ nm (41, 42). The PB/PS bilayer samples will then be progressively annealed at 120 °C for an extended period of time t_a (up to 100 min). This progressive annealing at an elevated temperature above the T_g^{bulk} of both layers allows the PB/PS polymer-polymer interface to form, reaching an equilibrium interfacial width of $w_I \approx 5$ nm, based on neutron reflectivity measurements by Genzer and Composto (41, 43) in agreement with literature χ values (44). From previous fluorescence measurements, we believe the PB/PS bilayer initially held at only 25 °C has a sharp $T_g(z)$ profile, similar to the composition profile, that then broadens on annealing at 120 °C to the $T_g(z)$ profile shown in Fig. 1A (7–9). As such, we might anticipate that the PB/PS bilayer initially held at only 25 °C ($t_a = 0$) would also have a sharp $\widetilde{G}(z)$ profile that might then also broaden on annealing at 120 °C. This is what we seek to test using a continuum physics analysis for the QCM shear wave propagation across the sample.

We start by comparing in Fig. 2 the resonance traces for the $n = 1$ and $n = 7$ harmonics for a PB/PS bilayer sample, composed of a PB layer of thickness $h_{\text{PB}} = 360$ nm atop a PS layer of thickness $h_{\text{PS}} = 1100$ nm supported on the QCM sensor, collected prior to and after annealing at 120 °C for 100 min. The thicknesses of the PB and PS layers separately measured by ellipsometry were 306 ± 2 nm and 1170 ± 70 nm, respectively, in reasonable agreement with the layer thicknesses determined by the QCM continuum physics model. The initial traces (blue curves) were collected on a PB/PS

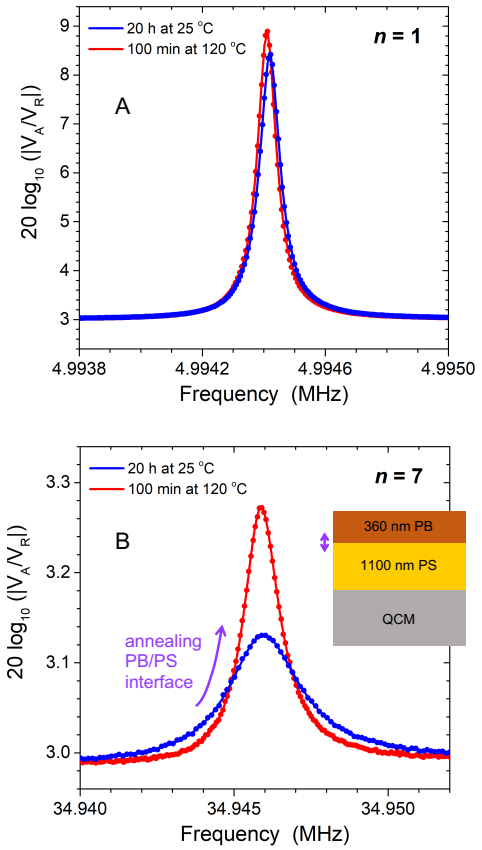

Fig. 2: Resonance frequency traces of a PB/PS bilayer collected after initially only being held at 25 °C for 20 h (blue curves) and after annealing at 120 °C for 100 min (red curves). (A) The $n = 1$ ($f_0 = 5$ MHz) resonance displays only a small shift on annealing because the QCM is primarily sensitive to the film's mass at this frequency, while (B) the $n = 7$ (35 MHz) resonance demonstrates a strong decrease in dissipation Γ_7 (becomes more narrow) with annealing at 120 °C due to increased transmission of the shear wave across the annealed PB/PS interface.

bilayer that was first held at 25 °C for 20 h under vacuum simply to consolidate the bilayer and remove any air gaps, giving a PB/PS interfacial width of $w_I \approx 1$ nm. The sample was then annealed for 100 min at 120 °C increasing the interfacial width to $w_I \approx 5$ nm (red curves). The fundamental $n = 1$ harmonic is primarily sensitive to added mass, corresponding to the total bilayer thickness $h_{\rm PB} + h_{\rm PS}$ and its density ρ. As the PB/PS interface forms, there will be a small change in the total bilayer thickness and density associated with the local intermixing of PB and PS at the polymer-polymer interface. We would anticipate little change in the $n = 1$ resonance peak due to this process, which is confirmed by the data shown in Fig. 2A. The resonance frequency f_1 shifts only from $f_1 = 4.99442$ MHz $\pm$ 0.06 Hz to $f_1 = 4.99441$ MHz $\pm$ 0.06 Hz on annealing at 120 °C for 100 min, and the dissipation Γ_1 changes only from $\Gamma_1 = (26.65 \pm 0.06)$ Hz to $\Gamma_1 = (29.82 \pm 0.06)$ Hz, where the errors quoted here and elsewhere represent one standard deviation for the best fit values of f_n and Γ_n.

In contrast, at higher harmonics beyond the Sauerbrey regime, where the QCM is sensitive to the viscoelastic properties of the PB/PS bilayer (37, 45), a pronounced evolution to a sharper resonance (smaller dissipation) is observed on annealing at 120 °C. The $n = 7$ resonance peak shown in Fig. 2B was the highest harmonic collected for this sample, making it the most sensitive to changes in the viscoelastic properties of the PB/PS bilayer. The dissipation of the $n = 7$ harmonic decreases by nearly 50% from $\Gamma_7 = (1355 \pm 5)$ Hz to $\Gamma_7 = (692 \pm 2)$ Hz on annealing at 120 °C, even though the resonance frequency f_7 shows barely any shift from $f_7 = 34.94588$ MHz $\pm$ 6 Hz to $f_7 = 34.94585$ MHz $\pm$ 2 Hz. This large decrease in dissipation at higher harmonics is indicative of increased shear wave transmission across the PB/PS interface on annealing at 120 °C and a greater mechanical coupling between the layers. The resonance traces demonstrate that a large change in the viscoelastic properties of the PB/PS bilayer is occurring with this small increase in interfacial width w_I on annealing at 120 °C.

Continuum physics model analysis

We can use a continuum physics layer model analysis to determine the modulus of the polymer layers added to the QCM sensor. To accomplish this, we start by first measuring the initial PS bottom layer added to the QCM sensor. Following directly from our previous work (37), we fit the measured data of the resonance frequency $\Delta f(n)$ and dissipation $\Delta\Gamma(n)$ shifts as a function of harmonic number n to a set of coupled equations that treats the continuum mechanics of shear wave propagation through the layers of the QCM-polymer film system. This set of coupled equations comes from solving for the shear wave displacement and stress in each layer subject to the boundary conditions of displacement and stress continuity at each interface (37, 46).

The shear wave displacement in each layer j is treated as a one-dimensional shear wave oscillating in the $\hat{y}$-direction and propagating across the layers in the $\hat{z}$-direction

$$\vec{u}_j(z,t) = e^{i\tilde{\omega}t}\left(A_j\, e^{-i\tilde{k}_j z} + B_{\rm j}\, e^{i\tilde{k}_j z}\right)\hat{y}, \qquad (1)$$

where A_j and B_j are the wave amplitudes of the forward propagating and reflected waves, respectively. The complex wave vector $\tilde{k}_j = 2\pi\tilde{f}/\tilde{c}_j$ depends on the material properties of each layer as the speed of sound $\tilde{c}_j = \sqrt{\widetilde{G}_j/\rho_j}$ is determined by the frequency-dependent complex modulus $\widetilde{G}_j(\tilde{\omega}) = G'_j(\tilde{\omega}) + iG''_j(\tilde{\omega})$ and density ρ_j of each layer. Assuming incompressibility and Hooke's law for the small shear displacements of the linear viscoelastic polymer, the relevant component of the stress tensor is given by $\sigma_{yz} = \widetilde{G}\,\frac{\partial u_y}{\partial z}$. This multilayer system is then solved by applying standard boundary

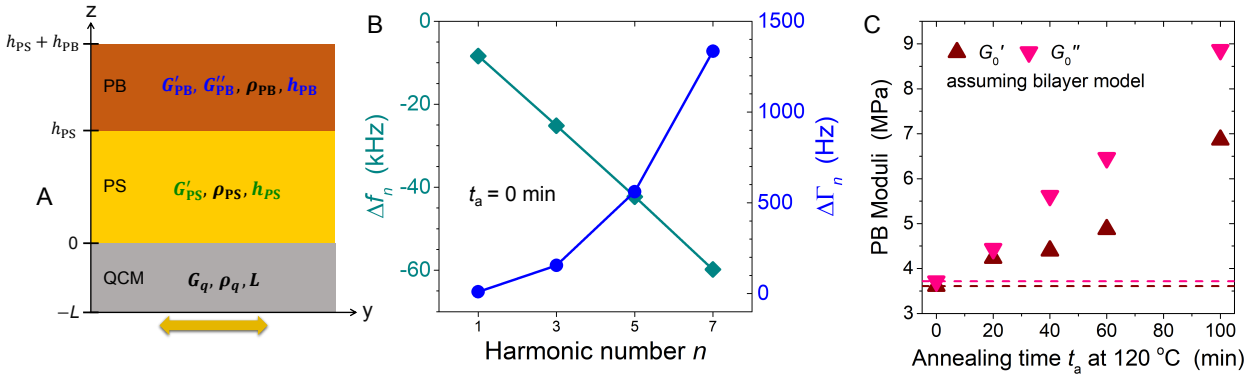

Fig. 3: (A) Schematic of continuum physics layer model geometry for PB/PS bilayer atop the QCM sensor with modulus, density, and thickness parameters of each layer indicated (parameters listed in blue are fit during the bilayer analysis, while parameters listed in green are fit during the single layer PS analysis). (B) Measured frequency $\Delta f(n)$ (teal diamonds) and dissipation $\Delta\Gamma(n)$ (blue circles) shifts as a function of harmonic number n for the PB/PS bilayer sample shown in Fig. 2 collected at $t_a = 0$ prior to annealing at 120 °C. Curves are fits to the $\Delta f(n)$ and $\Delta\Gamma(n)$ data using the bilayer continuum physics model as depicted in (A). (C) Change in modulus fit parameters, storage G'_{PB} and loss G''_{PB} for the PB layer as a function of annealing time t_a at 120 °C using the bilayer continuum physics model, demonstrating that the bilayer geometry as depicted in (A) becomes a poor model for the sample as the PB/PS interfacial width w_I grows on annealing. Dashed lines highlight the $G'_{PB} = 3.6$ MPa and $G''_{PB} = 3.7$ MPa values measured at $t_a = 0$ that are in good agreement with bulk PB modulus values (37).

conditions at each interface: continuity of displacement (no-slip) $\vec{u}_j(z,t)\big|_{z=j} = \vec{u}_{j+1}(z,t)\big|_{z=j}$ and stress continuity (Newton's third law) $\sigma_j(z,t)\big|_{z=j} = \sigma_{j+1}(z,t)\big|_{z=j}$, treating the top film/air and bottom quartz/air interfaces as stress free, $\sigma_j(z,t)\big|_{z=h,-L} = 0$. This leads to a set of coupled complex equations that can be solved numerically using standard methods (37).

To limit the number of fit parameters, the density of the polymer was held fixed at literature values: $\rho = 1.04$ g/cm^3 for PS (47) and $\rho = 0.895$ g/cm^3 for PB (48). In addition, the frequency-dependent shear modulus was treated as linear on a log-log scale, valid over the small frequency range of the QCM ($f_n = 5$–45 MHz) (38, 40), which for $f_n = nf_0 + \Delta f_n \approx nf_0$ gives (37):

$$G'(f_n) \approx G'(n) = G'_0\, n^{\beta'} \tag{2}$$

$$G''(f_n) \approx G''(n) = G''_0\, n^{\beta''} \tag{3}$$

This can be further simplified for glassy PS by recognizing that at room temperature for the MHz frequencies of the QCM, PS can be treated with simply a frequency-independent storage modulus $G'(f_n) = G'_{PS}$ (37). For rubbery PB, in its glass transition region at MHz frequencies, we must keep all terms, but can use literature rheology data to determine the exponents $\beta' = 0.50$ and $\beta'' = 0.74$ (37, 48, 49), leaving only the modulus prefactors G'_0 and G''_0, designated G'_{PB} and G''_{PB}, as fit parameters. Using this approach, we were able to successfully measure the frequency-dependent modulus of PS and PB single layer films using QCM at MHz frequencies, agreeing with literature rheometry data that was time-temperature shifted (37).

In the present work, we expand this continuum physics layer model analysis to accommodate PB/PS bilayer films atop the QCM sensor. Fig. 3A illustrates the bilayer model geometry of the PB layer atop the PS layer on the QCM sensor with the relevant parameters (modulus, density, thickness) of each layer listed. Compared to the single layer film case described previously (37), the bilayer case adds an additional layer and interface with boundary conditions at $z = h_{PS}$ between the PB and PS layers, as detailed in the Supplementary Information. The thickness h_{PS} and modulus G'_{PS} of the bottom PS layer are determined from an initial QCM measurement of the single layer PS film prior to adding the PB layer on top, and then subsequently held fixed for all bilayer analysis. This leaves three fitting parameters to be determined from an analysis of the bilayer measurements: the storage G'_{PB} and loss G''_{PB} modulus of the PB layer and its thickness h_{PB}.

Fig. 3B graphs the frequency $\Delta f(n)$ and dissipation $\Delta\Gamma(n)$ shifts measured for harmonic numbers $n = 1$–7 collected at $t_a = 0$ prior to annealing the PB/PS bilayer film at 120 °C for the 360 nm thick PB layer atop the 1100 nm thick PS layer sample whose resonance peaks are shown in Fig. 2A. At this stage prior to annealing at 120 °C, when the sample has only been held at 25 °C, the PB/PS interface is still sharp with an interfacial width $w_I \approx 1$ nm making the bilayer model geometry depicted in Fig. 3A an accurate representation for the sample. This is confirmed by the excellent fits of the QCM continuum physics bilayer model depicted in Fig. 3A to the $\Delta f(n)$ and $\Delta\Gamma(n)$ data, shown as the curves in Fig. 3B, with fit parameters $G'_{PB} = 3.6 \pm 0.5$ MPa, $G''_{PB} = 3.7 \pm 0.5$ MPa, and $h_{PB} = 362 \pm 18$ nm. The thickness and modulus of the PS layer $h_{PS} = 1098 \pm 4$ nm

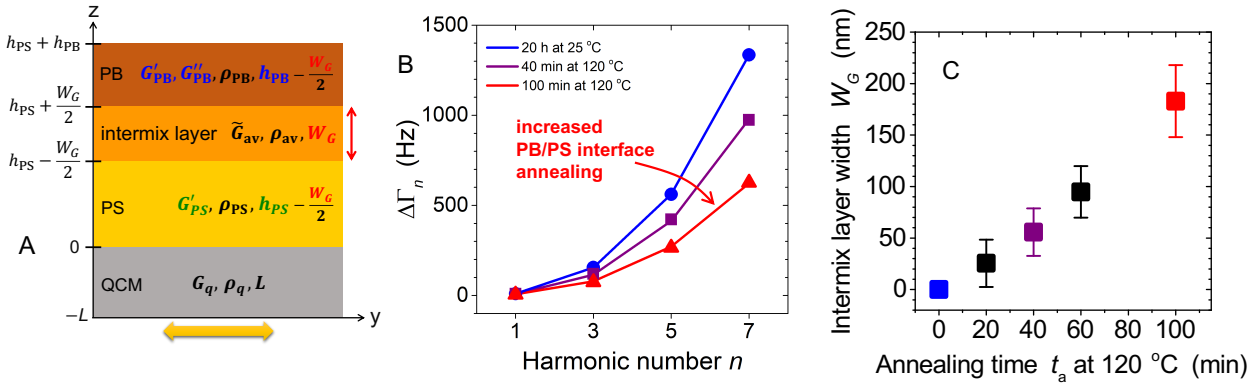

Fig. 4: (A) Schematic of trilayer geometry for QCM continuum physics model containing an intermix layer of average modulus $\widetilde{G}_{\rm av}$ and density $\rho_{\rm av}$ with thickness W_G between the PB and PS layers. Red symbols indicate fit parameters for the trilayer geometry, blue symbols indicate parameters determined from bilayer geometry fit at $t_a = 0$, and green symbols were parameters determined from fit to single layer PS film data. (B) Measured dissipation shift $\Delta\Gamma(n)$ as a function of harmonic number demonstrating the progressive decrease in dissipation with annealing time at 120 °C (symbols). Curves are fits of the QCM continuum physics model to $\Delta f(n)$ and $\Delta\Gamma(n)$ data using the bilayer geometry of Fig. 3A for the blue circles collected at $t_a = 0$ (after being held only at 25 °C for 20 h) and to the trilayer geometry of Fig. 4A for the data annealed at 120 °C for $t_a = 40$ min (purple squares) giving $W_G = 67$ nm and $t_a = 100$ min (red triangles) giving $W_G = 154$ nm. (C) Increase in the intermix layer thickness W_G corresponding to the width of the modulus gradient $\widetilde{G}(z)$ as a function of annealing time t_a at 120 °C. Symbols and error bars represent the average and standard deviation of W_G measured from three nominally identical samples.

and $G'_{\rm PS} = 2.0 \pm 0.2$ GPa were determined from the fit to the single layer PS film prior to adding the PB layer on top, and then subsequently held fixed during the fit to the bilayer geometry. These measured fit values agree well with the modulus values for bulk single layer films of these polymers measured previously: $G'_{\rm PB} = 3.3 \pm 0.6$ MPa, $G''_{\rm PB} = 4.4 \pm 0.3$ MPa, and $G'_{\rm PS} = 1.7 \pm 0.2$ GPa (37).

We now explore what happens to the parameters from the QCM bilayer model analysis upon annealing of the PB/PS bilayer film at 120 °C that acts to increase the PB/PS interfacial width w_I from ≈1 nm to ≈5 nm. As demonstrated in Fig. 1, this small increase in interfacial width w_I results in the development of a broad profile in local $T_{\rm g}(z)$ across the PB/PS interface with a $T_{\rm g}$-breadth $W_{T_{\rm g}} \approx 200$ nm (4, 7–9). If a correspondingly broad profile in local modulus $\widetilde{G}(z)$ also develops on annealing at 120 °C, we might expect the accuracy of the bilayer geometry to break down when fitting the QCM data. This breakdown is demonstrated by Fig. 3C that graphs the $G'_{\rm PB}$ and $G''_{\rm PB}$ fit parameters determined from applying the QCM bilayer analysis depicted in Fig. 3A as a function of annealing time t_a at 120 °C. The horizontal dash lines correspond to the best fit values of $G'_{\rm PB} = 3.6$ MPa and $G''_{\rm PB} = 3.7$ MPa obtained at $t_a = 0$ that are in good agreement with bulk PB modulus values (37). As shown by the graph, interpreting the data with this simple bilayer model results in modulus values for the PB layer that are on average more than double the bulk value, which seems unrealistic given what is known about the $T_{\rm g}(z)$ gradient in this system. We believe the simple bilayer model depicted in Fig. 3A, corresponding to a sharp change in modulus at the PB/PS interface, becomes a poor model for the PB/PS bilayer samples when annealed at 120 °C.

It has been well established in the literature that interfacial perturbations lead to depth-dependent gradients in property changes (1–5, 7–9, 14, 35). As such, we consider now a modified QCM continuum physics model that approximates a broad gradient in modulus $\widetilde{G}(z)$ between the PB and PS layers on annealing, which may mimic the broad $T_{\rm g}(z)$ gradient that has previously been measured for PB/PS bilayers. To keep the layer model simple and limit the number of additional fit parameters, we treat the annealed PB/PS bilayer sample with a trilayer geometry where we have inserted an intermix layer at the interface between the PB and PS layers, as depicted in Fig. 4A. For simplicity, we assume this intermix layer has a modulus and density corresponding to the average between that of PB and PS: $\widetilde{G}_{\rm av} = \frac{1}{2}(G_{\rm PB} + G'_{\rm PS})$ and $\rho_{\rm av} = \frac{1}{2}(\rho_{\rm PB} + \rho_{\rm PS})$. The only adjustable parameter of this layer is its thickness W_G corresponding to the width of the modulus profile $\widetilde{G}(z)$.

We approach fitting the data with this trilayer model by starting from the bilayer model fit depicted in Fig. 3A to the $\Delta f(n)$ and $\Delta\Gamma(n)$ data collected at $t_a = 0$ prior to any annealing at 120 °C. This bilayer fit to the $t_a = 0$ data defines the PB layer model parameters $G'_{\rm PB}$, $G''_{\rm PB}$, and $h_{\rm PB}$, while $G'_{\rm PS}$ and $h_{\rm PS}$ were already determined from the fit to the single layer PS film. We then fix all these parameters, allowing only the width of the intermix layer W_G to vary for fitting the trilayer model of Fig. 4A to the $\Delta f(n)$ and $\Delta\Gamma(n)$ data with $t_a > 0$ annealed at 120 °C.

Fig. 4B plots the measured dissipation shifts $\Delta\Gamma(n)$ over the harmonic range $n = 1$ to 7 for different annealing times $t_a = 0$, 40, and 100 min at 120 °C. A progressive decrease in dissipation is observed, especially at higher harmonics that are most sensitive to the viscoelastic properties of the PB/PS bilayer film, resulting from the small increase in PB/PS interfacial width w_I from approximately 1 to 5 nm with annealing. The corresponding frequency shifts $\Delta f(n)$ show little change with annealing as was demonstrated by the resonance peaks in Fig. 2. The curves in Fig. 4B correspond to fits of the QCM continuum physics model to the $\Delta f(n)$ and $\Delta\Gamma(n)$ data. The $t_a = 0$ data held only at 25 °C for 20 h was fit to the bilayer model of Fig. 3A, determining the parameter values for the PB and PS layers. The $t_a = 40$ and 100 min data annealed at 120 °C were then fit to the trilayer model of Fig. 4A holding the PB and PS layer parameters fixed, but allowing the thickness W_G of the intermix layer with average modulus $\widetilde{G}_{\rm av}$ and density $\rho_{\rm av}$ to vary. These fits to the trilayer data gave intermix layer thicknesses of $W_G = 67 \pm 23$ nm at $t_a = 40$ min and $W_G = 154 \pm 24$ nm at $t_a = 100$ min for this PB/PS bilayer sample of 360 nm of PB atop 1100 nm of PS. As discussed in Supplementary Information, we find the best fit W_G values to be robust to any reasonable average modulus $\widetilde{G}_{\rm av}$ value.

Fig. 4C plots the intermix thicknesses W_G as a function of annealing time t_a at 120 °C, where the data shown correspond to the average and standard deviation measured from three different samples with comparable PB and PS layer thicknesses. We consistently observe an increase in the intermix thickness up to $W_G \approx 180$ nm after 100 min of annealing demonstrating the development of a broad profile in modulus $\widetilde{G}(z)$ across the PB/PS interface. The $W_G \approx 180$ nm width of this broad modulus profile is comparable in size to the breadth of the $T_{\rm g}(z)$ profile ($W_{T_{\rm g}} \approx 200$ nm) that was observed previously for this PB/PS system (9).

We note that with this simplified trilayer model, we are unable to comment on whether there is an asymmetry to the modulus gradient, as was observed for the $T_{\rm g}(z)$ gradient. In fitting the data, we assume the total thickness of the bilayer film $h_{\rm PS} + h_{\rm PB}$ remains constant with annealing at 120 °C, where the thickness of the intermix layer W_G is treated as coming equally from the PS and PB layers. Future efforts will incorporate a more sophisticated QCM layer model that treats the depth dependent modulus gradient $\widetilde{G}(z)$ as continuous.

Conclusions

In agreement with the recent reports of long-ranged ∼200 nm $T_{\rm g}(z)$ profiles measured experimentally across glassy-rubbery polymer-polymer interfaces formed to equilibrium (4, 7–9), we have experimentally demonstrated here another long-range effect, measuring that an equally broad ≈180 nm gradient in modulus $\widetilde{G}(z)$ emerges when the ≈5 nm polymer-polymer interface is formed between PS and PB. These experimental observations, along with other previous reports of long-ranged interfacial effects (4), suggest we are missing some key physics in the theoretical formulations modeling interfacial perturbations (3).

We propose that how acoustic waves propagate across nanoconfined or nanostructured systems, reflecting at or transmitting across interfaces, alters the VDoS near the boson peak influencing long-ranged interactions between quasilocalized soft collective modes effectively coupling density fluctuations of α-relaxation events and associated local properties over long distances. It is known and been experimentally observed that the presence of interfaces in nanoconfined systems alters the VDoS near the boson peak (27–32). QLEs of soft potential regions near the boson peak are hybridized with propagating sounds waves of comparable energy (20, 25, 26) (∼1 meV, $\lambda \sim 5$ nm in PS (21)). It is thus reasonable to expect that density fluctuations caused by these $\lambda \sim 5$ nm acoustic waves would facilitate α-relaxations (5, 50). In fact, recent theoretical work by Mei and Schweizer have causally connected α-relaxation events with the amplitude of long wavelength density fluctuations (51–53).

Such a mechanism of acoustic wave propagation coupling α-relaxations over long distances is consistent with the available experimental evidence provided here for a broad modulus profile $\widetilde{G}(z)$ and previously for broad $T_{\rm g}(z)$ profiles (4, 8, 11) that long-range gradients across glassy-rubbery polymer-polymer interfaces are only observed when the polymer-polymer interface w_I becomes ≈ 5 nm (4, 8). The transmission of acoustic waves with $\lambda \sim 5$ nm across such an interface would be expected to depend on the interfacial width and difference in modulus in an acoustic impedance matching manner. In this picture, it is the propagation of thermally-excited acoustic waves of $\lambda \sim 5$ nm that are part of the existing VDoS near the boson peak that cause this long-range effect. One would expect such a mechanism to be present in bulk glasses, but likely not dominant as the acoustic waves and density fluctuations are on average equivalent across the system. Experimentally, we have made the phenomenon strongly visible by placing a glassy and rubbery domain in contact in such a way that the relevant VDoS can be coupled between domains with strongly different bulk dynamics. Density fluctuations that are more likely to be prevalent in the rubbery domain can propagate across the broadened polymer-polymer interface in the form of acoustic waves with $\lambda \sim 5$ nm, interacting with QLEs in the glassy domain and further softening the potential at ∼300 GHz frequencies facilitating α-relaxations. This provides a mechanism for establishing long-ranged gradients in local glass transition $T_{\rm g}(z)$ and in turn local modulus $\widetilde{G}(z)$ at a range of frequencies, some of which are measurable by QCM. What controls the length scale of the $T_{\rm g}(z)$ and modulus $\widetilde{G}(z)$ gradients

is unclear, but we speculate this could be associated with the mean free path ℓ of the $\lambda \sim 5$ nm acoustic waves in each domain because ℓ can be quite long-ranged in glasses and would be expected to be larger in the glassy PS domain than in the rubbery PB domain (54), consistent with the asymmetry observed in the $T_g(z)$ profiles.

Materials and Methods

Polystyrene (PS) ($M_w = 650$ kg/mol, $M_w/M_n = 1.06$) was purchased from Pressure Chemical and used as received. Polybutadiene (PB) ($M_w = 375$ kg/mol, $M_w/M_n = 2.4$; 36% cis-1,4; 55% trans-1,4; 9% vinyl-1,2, as specified by the supplier) was purchased from Scientific Polymer Products and washed three times by dissolving in tetrahydrofuran (THF) and precipitating in chilled methanol (9). The PS layer was spin-coated directly from a toluene solution onto the QCM sensor, as well as silicon pieces for film thickness determination by ellipsometry. Analysis of the $\Psi(\lambda)$ and $\Delta(\lambda)$ ellipsometry data for wavelengths spanning 400–1000 nm was done using an optical layer model with a Cauchy layer, $n(\lambda) = A + B/\lambda^2 + C/\lambda^4$, for the polymer film and a semi-infinite silicon substrate with a 1.25 nm native oxide layer, as previously described (37).

The PS film on the QCM was annealed under vacuum for a minimum of 14 h at a temperature of 120 °C to remove residual solvent and release stresses developed during spin-coating. QCM measurements were then collected on this PS film to determine the film thickness using the continuum physics model (37). The PB layer was spin-coated from a toluene solution onto freshly-cleaved mica, then immediately floated onto room temperature deionized water and captured from below with the annealed PS layer atop the QCM. The PB/PS bilayer was then placed in a 25 °C vacuum oven for 20 h to relax the PB film and remove any air gaps between the PB and PS layers. QCM measurements were then collected before and after annealing the bilayer in a vacuum oven for different annealing times t_a at 120 °C.

Measurements of the QCM resonance peak at different harmonic numbers n for the PS single layer and PB/PS bilayer films were collected at room temperature (25 °C) using AT-cut quartz sensors from Stanford Research systems with a fundamental frequency f_0 of 5 MHz using an Agilent 4395a vector network analyzer at 0 dBm, corresponding to a source power of 1 mW (37). An analytical fitting function determined from the circuit model for the QCM setup was used to fit the data for each resonance peak to obtain the resonance frequency f_n and dissipation Γ_n at the fundamental frequency $n = 1$ of the quartz oscillation and higher odd harmonics n, as described in Ref. (37). The bare quartz resonance frequency and dissipation measured at each harmonic number prior to adding of the film were subtracted from the film-loaded values to obtain the frequency and dissipation shifts $\Delta f_n = f_n^{\text{film+QCM}} - f_n^{\text{bare QCM}}$ and $\Delta\Gamma_n = \Gamma_n^{\text{film+QCM}} - \Gamma_n^{\text{bare QCM}}$. The moduli and thicknesses of the PB and PS layers were then determined by analyzing the frequency $\Delta f(n)$ and dissipation $\Delta\Gamma(n)$ shifts as a function of harmonic number n using a continuum physics model to describe the shear wave propagation across the multiple layers of the QCM-film system. The continuum physics model has been previously described in Ref. (37), and in the Supplementary Information we outline its extension to bilayer and trilayer films.

ACKNOWLEDGMENTS

The authors gratefully acknowledge useful discussions with Alexander Couturier, Eric Weeks and Daniel Sussman, in addition to support from the National Science Foundation Polymers Program (DMR-1905782) and Emory University.

1. S. Butler, P. Harrowell, Glassy relaxation at surfaces: The correlation length of cooperative motion in the facilitated kinetic Ising model. *Journal of Chemical Physics* **95**, 4466 – 4470 (1991).
2. C. J. Ellison, J. M. Torkelson, The distribution of glass-transition temperatures in nanoscopically confined glass formers. *Nature Materials* **2**, 695 – 700 (2003).
3. K. S. Schweizer, D. S. Simmons, Progress towards a phenomenological picture and theoretical understanding of glassy dynamics and vitrification near interfaces and under nanoconfinement. *Journal of Chemical Physics* **151**, 240901 (2019).
4. C. B. Roth, Polymers under nanoconfinement: Where are we now in understanding local property changes? *Chemical Society Reviews* **50**, 8050–8066 (2021).
5. N. B. Tito, J. E. G. Lipson, S. T. Milner, Lattice model of mobility at interfaces: free surfaces, substrates, and bilayers. *Soft Matter* **9**, 9403 – 9413 (2013).
6. W. Zhang, F. W. Starr, J. F. Douglas, Activation free energy gradient controls interfacial mobility gradient in thin polymer films. *Journal of Chemical Physics* **155**, 174901 (2021).
7. R. R. Baglay, C. B. Roth, Communication: Experimentally determined profile of local glass transition temperature across a glassy-rubbery polymer interface with a Tg difference of 80 K. *Journal of Chemical Physics* **143**, 111101 (2015).
8. R. R. Baglay, C. B. Roth, Local glass transition temperature Tg(z) of polystyrene next to different polymers: Hard vs. soft confinement. *Journal of Chemical Physics* **146**, 203307 (2017).
9. B. L. Kasavan, R. R. Baglay, C. B. Roth, Local Glass Transition Temperature Tg(z) Profile in Polystyrene next to Polybutadiene with and without Plasticization Effects. *Macromolecular Chemistry And Physics* **219**, 1700328 (2018).
10. R. A. L. Jones, R. W. Richards, *Polymers at Surfaces and Interfaces*. (Cambridge University Press, Cambridge, UK), (1999).
11. Y. J. Gagnon, C. B. Roth, Local Glass Transition Tem-

perature Tg(z) Within Polystyrene Is Strongly Impacted by the Modulus of the Neighboring PDMS Domain. *ACS Macro Letters* **9**, 1625–1631 (2020).

12. J. Wang, G. B. McKenna, A novel temperature-step method to determine the glass transition temperature of ultrathin polymer films by liquid dewetting. *Journal of Polymer Science Part B: Polymer Physics* **51**, 1343–1349 (2013).
13. R. J. Lang, W. L. Merling, D. S. Simmons, Combined dependence of nanoconfined Tg on interfacial energy and softness of confinement. *ACS Macro Letters* **3**, 758 – 762 (2014).
14. A. Ghanekarade, D. S. Simmons, Combined Mixing and Dynamical Origins of Tg Alterations Near Polymer–Polymer Interfaces. *Macromolecules* **56**, 379–392 (2023).
15. M. Shimada, H. Mizuno, A. Ikeda, Anomalous vibrational properties in the continuum limit of glasses. *Physical Review E* **97**, 022609 (2018).
16. J. E. Pye, C. E. Wood, J. C. Burton, Precursors to Molecular Slip on Smooth Hydrophobic Surfaces. *Physical Review Letters* **121**, 134501 (2018).
17. R. C. Zeller, R. O. Pohl, Thermal Conductivity and Specific Heat of Noncrystalline Solids. *Physical Review B* **4**, 2029 – 2041 (1971).
18. W. A. Phillips, ed., *Amorphous Solids: Low-Temperature Properties*. (Springer-Verlag, Berlin) Vol. 24 Topics in Current Physics, (1981).
19. T. S. Grigera, V. Martín-Mayor, G. Parisi, P. Verrocchio, Phonon interpretation of the 'boson peak' in supercooled liquids. *Nature* **422**, 289–292 (2003).
20. E. Lerner, E. Bouchbinder, Low-energy quasilocalized excitations in structural glasses. *Journal of Chemical Physics* **155**, 200901 (2021).
21. U. Buchenau, C. Pecharroman, R. Zorn, B. Frick, Neutron Scattering Evidence for Localized Soft Modes in Amorphous Polymers. *Physical Review Letters* **77**, 659–662 (1996).
22. A. Widmer-Cooper, H. Perry, P. Harrowell, D. R. Reichman, Irreversible reorganization in a supercooled liquid originates from localized soft modes. *Nature Physics* **4**, 711–715 (2008).
23. M. L. Manning, A. J. Liu, Vibrational Modes Identify Soft Spots in a Sheared Disordered Packing. *Physical Review Letters* **107**, 108302 (2011).
24. A. Smessaert, J. Rottler, Structural Relaxation in Glassy Polymers Predicted by Soft Modes: A Quantitative Analysis. *Soft Matter* **10**, 8533–8541 (2014).
25. E. Lerner, E. Bouchbinder, Boson-peak vibrational modes in glasses feature hybridized phononic and quasilocalized excitations. *Journal of Chemical Physics* **158**, 194503 (2023).
26. U. Buchenau, Y. M. Galperin, V. L. Gurevich, D. A. Parshin, M. A. Ramos, H. R. Schober, Interaction of soft modes and sound waves in glasses. *Physical Review B* **46**, 2798–2808 (1992).
27. T. S. Jain, J. J. de Pablo, Influence of confinement on the vibrational density of states and the Boson peak in a polymer glass. *Journal of Chemical Physics* **120**, 9371–9375 (2004).
28. R. Zorn, Boson peak in confined disordered systems. *Physical Review B* **81**, 054208 (2010).
29. R. Zorn, M. Mayorova, D. Richter, B. Frick, Inelastic neutron scattering study of a glass-forming liquid in soft confinement. *Soft Matter* **4**, 522–533 (2008).
30. R. Zorn, B. Frick, L. Hartmann, F. Kremer, A. Schönhals, D. Richter, Dynamics of confined glass-forming systems observed by neutron scattering. *Physica B: Condensed Matter* **350**, E1115–E1118 (2004).
31. R. Zorn, L. Hartmann, B. Frick, D. Richter, F. Kremer, Inelastic neutron scattering experiments on the dynamics of a glass-forming material in mesoscopic confinement. *Journal of Non-Crystalline Solids* **307**, 547–554 (2002).
32. R. Inoue, T. Kanaya, K. Nishida, I. Tsukushi, K. Shibata, Inelastic Neutron Scattering Study of Low Energy Excitations in Polymer Thin Films. *Physical Review Letters* **95**, 056102 (2005).
33. K. Attenborough, M. Postema, *A pocket-sized introduction to acoustics*. (University of Hull), (2008).
34. V. T. Rathod, A Review of Acoustic Impedance Matching Techniques for Piezoelectric Sensors and Transducers. *Sensors* **20**, 4051 (2020).
35. B. D. Vogt, Mechanical and viscoelastic properties of confined amorphous polymers. *Journal of Polymer Science Part B: Polymer Physics* **56**, 9–30 (2018).
36. C. B. Roth, ed., *Polymer Glasses*. (CRC Press, Boca Raton, FL), (2016).
37. Y. J. Gagnon, J. C. Burton, C. B. Roth, Physically intuitive continuum mechanics model for quartz crystal microbalance: Viscoelasticity of rubbery polymers at MHz frequencies. *Journal of Polymer Science* **60**, 244–257 (2022).
38. D. Johannsmann, *The Quartz Crystal Microbalance in Soft Matter Research: Fundamentals and Modeling*. (Springer International Publishing, Switzerland), (2015).
39. D. Johannsmann, A. Langhoff, C. Leppin, Studying Soft Interfaces with Shear Waves: Principles and Applications of the Quartz Crystal Microbalance (QCM). *Sensors* **21**, 3490 (2021).
40. K. R. Shull, M. Taghon, Q. Wang, Investigations of the high-frequency dynamic properties of polymeric systems with quartz crystal resonators. *Biointerphases* **15**, 021012 (2020).
41. J. Genzer, R. J. Composto, The interface between immiscible polymers studied by low-energy forward recoil spectrometry and neutron reflectivity. *Polymer* **40**, 4223–4228 (1999).
42. J. A. Forrest, K. Dalnoki-Veress, Sub-glass-transition temperature interface formation between an immiscible glass rubber pair. *Journal of Polymer Science Part B: Polymer Physics* **39**, 2664–2670 (2001).
43. E. J. Kramer, Depth profiling methods that provide information complementary to neutron reflectivity. *Physica B: Condensed Matter* **173**, 189–198 (1991).
44. D. Rigby, J. L. Lin, R. J. Roe, Compatibilizing effect of random or block copolymer added to binary mixture of homopolymers. *Macromolecules* **18**, 2269–2273 (1985).
45. K. Sadman, C. G. Wiener, R. A. Weiss, C. C. White,

K. R. Shull, B. D. Vogt, Quantitative Rheometry of Thin Soft Materials Using the Quartz Crystal Microbalance with Dissipation. *Analytical Chemistry* **90**, 4079–4088 (2018).

46. B. Lautrup, *Physics of Continuous Matter*. (CRC Press, Boca Raton, FL), 2 edition, (2011).
47. J. Brandrup, E. H. Immergut, E. A. Grulke, A. Abe, D. H. Bloch, eds., *Polymer Handbook*. (Wiley, New York), 4th edition, (1999).
48. R. H. Colby, L. J. Fetters, W. W. Graessley, The melt viscosity-molecular weight relationship for linear polymers. *Macromolecules* **20**, 2226–2237 (1987).
49. S. J. Park, P. S. Desai, X. Chen, R. G. Larson, Universal Relaxation Behavior of Entangled 1,4-Polybutadiene Melts in the Transition Frequency Region. *Macromolecules* **48**, 4122–4131 (2015).
50. R. P. White, J. E. G. Lipson, Dynamics across a Free Surface Reflect Interplay between Density and Cooperative Length: Application to Polystyrene. *Macromolecules* **54**, 4136–4144 (2021).
51. B. Mei, Y. Zhou, K. S. Schweizer, Long Wavelength Thermal Density Fluctuations in Molecular and Polymer Glass-Forming Liquids: Experimental and Theoretical Analysis under Isobaric Conditions. *Journal of Physical Chemistry B* **125**, 12353–12364 (2021).
52. B. Mei, Y. Zhou, K. S. Schweizer, Experimental test of a predicted dynamics–structure–thermodynamics connection in molecularly complex glass-forming liquids. *Proceedings of the National Academy of Sciences* **118**, e2025341118 (2021).
53. B. Mei, Y. Zhou, K. S. Schweizer, Experimental Tests of a Theoretically Predicted Noncausal Correlation between Dynamics and Thermodynamics in Glass-forming Polymer Melts. *Macromolecules* **54**, 10086–10099 (2021).
54. R. O. Pohl, X. Liu, E. Thompson, Low-temperature thermal conductivity and acoustic attenuation in amorphous solids. *Reviews of Modern Physics* **74**, 991–1013 (2002).

SUPPLEMENTARY INFORMATION

Development of broad modulus profile upon polymer-polymer interface formation between immiscible glassy-rubbery domains

Yannic J. Gagnon, Justin C. Burton, Connie B. Roth

Department of Physics, Emory University, Atlanta, Georgia 30322 USA

Contact: cbroth@emory.edu

For *PNAS*, revised version dated October 2, 2023

Polybutadiene/Polystyrene Interfacial Width

The interfacial width that forms between high molecular weight polybutadiene (PB) and polystyrene (PS) polymers has been well studied by Genzer and Composto using both neutron reflectivity and low-energy forward recoil spectrometry (LE-FRES) (1). The molecular weights and PB microstructure used for their study of the PS/PB interfacial composition are comparable to those we use in the present study: PS with $M_{\mathrm{w}} = 575$ kg/mol ($M_{\mathrm{w}}/M_{\mathrm{n}} = 1.06$), deuterated PS (dPS) with $M_{\mathrm{w}} = 550$ kg/mol ($M_{\mathrm{w}}/M_{\mathrm{n}} = 1.05$), and PB with $M_{\mathrm{w}} = 270$ kg/mol ($M_{\mathrm{w}}/M_{\mathrm{n}} = 1.32$ and 49.8% cis-1,4, 43.5% trans-1.4, 6.7% vinyl-1,2). The interfacial width between PS and PB was studied both prior to and after high temperature annealing. The PB/PS bilayer samples were assembled by first spin-coating a ≈400 nm thick PB layer and annealing it overnight at 60 °C under vacuum. Then a ≈60 nm thick layer of dPS or PS/dPS mixture was floated atop the PB layer. The assembled PS/PB bilayer was then held at 50 °C overnight under vacuum. This initial sample without any high temperature annealing was measured showing an initial PS/PB interface roughness of 1.5 nm by neutron reflectivity (1). As experimental measurements of interfacial width reflect both the true local interfacial width and interface roughness averaged over the area of the sample probed by the measurement beam, the actual interfacial width would be expected to be less than this, especially for the initial state of the bilayer (1, 2). Forrest and Dalnoki-Veress demonstrated that limited interfacial broadening occurs between rubbery and glassy polymers until temperatures above the T_{g} of the glassy component are reached (3). Thus for our initial PB/PS bilayers, held at only 25 °C for 20 hours, we would not expect the PB/PS interfacial width to be more than ≈1 nm.

In the Genzer and Composto study, their PS/PB bilayers were then annealed for 4 days at 175 °C giving a broadened interfacial width of 3.6 nm (1). The reported volume fraction profiles determined from

neutron reflectivity show that the full span of the PS/PB interface is ≈5 nm. These values were shown to be in good agreement with self-consistent field theory calculations in the limit of infinite molecular weight using literature values of the PS/PB χ interaction parameter (1, 4). The measured interfacial widths from LE-FRES on samples that were annealed for 7 days at 175 °C were found to be comparable at 6.0 ± 3.5 nm, but slightly larger in both magnitude and error because this experimental technique has a depth resolution of only 13 nm, in contrast to neutron reflectivity's depth resolution that is better than 1 nm (1). The LE-FRES measurements do provide good confirmation that the PS/PB interfacial width spans no larger than ≈25 nm, ensuring that the neutron reflectivity analysis is not missing some small gradual change in composition further from the interface (5). Using mixtures of PS and dPS for the neutron reflectivity measurements, Genzer and Composto also confirmed that deuteration had no significiant impact on the PS/PB interaction (1).

The PS and PB molecular weights used in our present study are slightly higher than those used by Genzer and Composto, but this should have little to no impact on the interfacial width as the molecular weights used in the Genzer and Composto study are already well within the high molecular weight limit (1). The PS/PB interaction parameter χ is weakly temperature dependent such that at our annealing temperature of 120 °C, χ would be slightly larger suggesting a narrower interfacial width by ≈0.2 nm compared with that measured at 175 °C (1, 4). Thus, we conclude that the PB/PS bilayer broadens to ≈5 nm after annealing at 120 °C. The time scale of polymer-polymer interface formation of PS/dPS bilayers at 120 °C takes about 100 min to reach a 5 nm interfacial width (2), where we would expect the time scale for PB/PS interfaces to be comparable or perhaps slightly faster (3, 6).

The probability that some low molecular weight component is migrating across the interface to mix with the other component is extremely unlikely as our PB was washed three times to remove the small molecule antioxidant that is typically added to PB, which would also wash away the very low molecular weight part of the PB distribution. Our high molecular weight PS was anionically synthesized, meaning no low molecular weight component is present in its distribution. Even though PS and PB can be miscible at very low, oligomeric molecular weights (≈2 kg/mol) (7), polymers become strongly immiscible with increasing molecular weight. Roe and Zin demonstrated that the upper critical solution temperature (UCST) increases from ≈150 °C to already ≈220 °C just increasing the PS molecular weight from M_w = 2.4 kg/mol to M_w = 3.5 kg/mol when mixed with PB of M_w = 2.6 kg/mol with comparable microstructure to our own PB (8). Our molecular weights of PS M_w = 650 kg/mol and PB M_w = 375 kg/mol are more than two orders of magnitude higher and thus would not be miscible at any temperature.

Continuum Physics Model Analysis of the QCM-film System

The continuum physics layer model used here to fit the Δf_n and $\Delta\Gamma_n$ experimental data is an extension from that developed recently in Ref. (9). The QCM produces a shear wave that obeys the boundary conditions of continuity of stress and displacement across the layers, and zero stress boundary conditions at the free surfaces. These continuity equations are numerically solved for the frequency and dissipation shifts $\Delta f(n)$ and $\Delta\Gamma(n)$ at each odd harmonic n. To compute the Δf_n and $\Delta\Gamma_n$ values, we treat the QCM system as undriven such that it acts as an underdamped harmonic oscillator with the amplitude of motion decreasing exponentially in time. This simplifies the data analysis because the frequency and dissipation can be combined into a complex frequency $\widetilde{\omega} = 2\pi\tilde{f} = 2\pi(nf_0 + \Delta f_n + i\Delta\Gamma_n)$. The essential ingredients of the model are that the QCM and polymer layers atop the QCM are treated as continuum layers described by a complex, frequency-dependent shear modulus $\widetilde{G}(f) = G'(f) + i\,G''(f)$, density ρ, and film thickness h. The density is held constant at a value determined from the literature.

For the specific cases of PS and PB, the modulus of PS at room temperature and MHz frequencies is approximately constant and can be well fit by a single frequency independent storage modulus parameter $G'_{\rm PS}$ (9). The density of PS is held fixed at $\rho = 1.04$ g/cm^3 (9, 10). The modulus of PB at room temperature and in the frequency range between 5 MHz to 45 MHz (corresponding to the QCM harmonic range of $n = 1$ to 9) was previously established to depend on the harmonic number (frequency) as $\widetilde{G}(f) = G'(f) + i\,G''(f) = G'_0\,n^{\beta'} + i\,G''_0\,n^{\beta''}$ (9). The values for the storage modulus exponent β' and the loss modulus exponent β'' were determined in Ref. (9) by fitting literature data for PB to obtain $\beta' = 0.50 \pm 0.03$ and $\beta'' = 0.74 \pm 0.01$, where excellent agreement was found between the storage and loss moduli for PB determined by QCM with that from literature studies that were collected by rheometry at lower frequency then time-temperature shifted to MHz frequencies at a 25 °C reference temperature. The density of PB is held fixed at $\rho = 0.895$ g/cm^3 (9, 11).

We define our axes such that the shear wave produced by the QCM is treated as propagating in the $\hat{z}$-direction and oscillating in the $\hat{y}$-direction (9). The shear displacement and shear stress in a given layer j are given by:

$$\vec{u}_j(z,t) = e^{i\widetilde{\omega}t}\left(A_j\,e^{-i\tilde{k}_j z} + B_j\,e^{i\tilde{k}_j z}\right)\hat{y} \tag{S1}$$

$$\sigma_j = \widetilde{G}_j\,\frac{\partial u_j}{\partial z}\,, \tag{S2}$$

where σ_{yz} is the only nonzero component of the stress tensor, $\tilde{k}_j = 2\pi\tilde{f}/\tilde{c}_j$ is the complex wave vector, and A_j and B_j are the wave amplitudes of the forward propagating and reflected waves, respectively. The

complex angular frequency $\widetilde{\omega}$ at a given harmonic number n is related to the frequency and dissipation shifts by $\widetilde{\omega} = 2\pi\widetilde{f} = 2\pi(nf_0 + \Delta f_n + i\Delta\Gamma_n)$.

For the PB/PS bilayer model shown in Fig. 3A, continuity of displacement at the PS/quartz interface at $z = 0$ (no-slip boundary condition) gives

$$\begin{aligned} u_{\mathrm{PS}}(z,t)\Big|_{z=0} &= u_{\mathrm{q}}(z,t)\Big|_{z=0} \\ A_{\mathrm{PS}} + B_{\mathrm{PS}} &= A_{\mathrm{q}} + B_{\mathrm{q}}\,, \end{aligned} \tag{S3}$$

and continuity of displacement at the PB/PS interface ($z = h_{\mathrm{PS}}$) gives

$$\begin{aligned} u_{\mathrm{PB}}(z,t)\Big|_{z=h_{\mathrm{PS}}} &= u_{\mathrm{PS}}(z,t)\Big|_{z=h_{\mathrm{PS}}} \\ A_{\mathrm{PB}}\, e^{-i\widetilde{k}_{\mathrm{PB}}h_{\mathrm{PS}}} + B_{\mathrm{PB}}\, e^{i\widetilde{k}_{\mathrm{PB}}h_{\mathrm{PS}}} &= A_{\mathrm{PS}}\, e^{-ik_{\mathrm{PS}}h_{\mathrm{PS}}} + B_{\mathrm{PS}}\, e^{ik_{\mathrm{PS}}h_{\mathrm{PS}}}\,. \end{aligned} \tag{S4}$$

Stress continuity (Newton's third law) at the PS/quartz interface ($z = 0$) gives

$$\begin{aligned} \sigma_{\mathrm{PS}}(z,t)\Big|_{z=0} &= \sigma_{\mathrm{q}}(z,t)\Big|_{z=0} \\ \sqrt{\rho_{\mathrm{PS}}\, G'_{\mathrm{PS}}}\,(A_{\mathrm{PS}} - B_{\mathrm{PS}}) &= Z_{\mathrm{q}}\,(A_{\mathrm{q}} - B_{\mathrm{q}})\,, \end{aligned} \tag{S5}$$

where $\sqrt{\rho_{\mathrm{PS}}\, G'_{\mathrm{PS}}}$ is the acoustic impedance of PS, and Z_{q} is the known acoustic impedance for AT-cut quartz: $Z_{\mathrm{q}} = \sqrt{\rho_{\mathrm{q}}\, G_{\mathrm{q}}} = 8.8 \times 10^9$ g m^{-2} Hz (9, 12). The relation $k = \frac{\omega}{c} = \omega\sqrt{\frac{\rho}{G}}$ was used to substitute for the wavevector prefactors that are gained after taking derivatives of the displacement. Stress continuity at the PB/PS interface ($z = h_{\mathrm{PS}}$) gives

$$\begin{aligned} \sigma_{\mathrm{PB}}(z,t)\Big|_{z=h_{\mathrm{PS}}} &= \sigma_{\mathrm{PS}}(z,t)\Big|_{z=h_{\mathrm{PS}}} \\ \sqrt{\rho_{\mathrm{PB}}\,\widetilde{G}_{\mathrm{PB}}}\left[A_{\mathrm{PB}}\, e^{-i\widetilde{k}_{\mathrm{PB}}h_{\mathrm{PS}}} - B_{\mathrm{PB}}\, e^{i\widetilde{k}_{\mathrm{PB}}h_{\mathrm{PS}}}\right] &= \sqrt{\rho_{\mathrm{PS}}\, G'_{\mathrm{PS}}}\,\left[A_{\mathrm{PS}}\, e^{-ik_{\mathrm{PS}}h_{\mathrm{PS}}} - B_{\mathrm{PS}}\, e^{ik_{\mathrm{PS}}h_{\mathrm{PS}}}\right]\,, \end{aligned} \tag{S6}$$

where $\sqrt{\rho_{\mathrm{PB}}\,\widetilde{G}_{\mathrm{PB}}}$ is the acoustic impedance of PB. The PB film/air and bottom quartz/air interfaces are stress-free, giving

$$\begin{aligned} \sigma_{\mathrm{PB}}(z,t)\Big|_{z=(h_{\mathrm{PS}}+h_{\mathrm{PB}})} &= 0 \\ A_{\mathrm{PB}} - B_{\mathrm{PB}}\,\exp\left[i4\pi(h_{\mathrm{PS}} + h_{\mathrm{PB}})\sqrt{\frac{\rho_{\mathrm{PB}}}{\widetilde{G}_{\mathrm{PB}}}}\,(f_n + i\Gamma_n)\right] &= 0\,, \end{aligned} \tag{S7}$$

and

$$\sigma_{\rm q}(z,t)\Big|_{z=-L} = 0$$
$$A_{\rm q} - B_{\rm q}\,\exp\left[-i\frac{2\pi}{f_0}\,(f_n + i\Gamma_n)\right] = 0, \tag{S8}$$

where the thickness L of the quartz is related to the fundamental frequency f_0 by $L = \frac{\lambda_0}{2} = \frac{c_q}{2f_0}$.

To solve Equations (S3)-(S8), we first normalized the amplitudes by setting $A_{\rm q} = 1$. The PS film thickness $h_{\rm PS}$ and modulus $G'_{\rm PS}$ were determined from initial QCM measurements on the single-layer PS film prior to adding the PB layer on top and then held fixed during the bilayer analysis. Starting from initial guesses for the PB modulus $\widetilde{G}_{\rm PB} = G'_{\rm PB}\,n^{\beta'} + i\,G''_{\rm PB}\,n^{\beta''}$ and thickness $h_{\rm PB}$, the experimental $\Delta f(n)$ and $\Delta\Gamma(n)$ data for the QCM bilayer measurements were fit to the continuum physics model by performing chi-squared minimization using the local minimization routine FindMinimum in Mathematica, which performs a Levenberg-Marquardt algorithm. For a given harmonic number n, the Equations (S3)-(S8) (6 equations) were solved numerically for the six unknowns, all of which are complex: $\Delta\widetilde{f}_n = \Delta f_n + i\Delta\Gamma_n$, $B_{\rm q}$, $A_{\rm PS}$, $B_{\rm PS}$, $A_{\rm PB}$, $B_{\rm PB}$. The resulting best fit parameters from the bilayer analysis were the storage $G'_{\rm PB}$ and loss $G''_{\rm PB}$ moduli prefactors and film thickness $h_{\rm PB}$ of the PB layer.

For the trilayer model shown in Fig. 4A, the intermix layer is added in the same manner by applying the boundary conditions of stress and displacement continuity at $z = h_{\rm PS} + \frac{W_G}{2}$ and $z = h_{\rm PS} - \frac{W_G}{2}$ such that intermix layer thickness W_G comes equally from both the PS and PB layers, thus keeping the total film thickness $h_{\rm PS} + h_{\rm PB}$ constant. Fitting of the $\Delta f(n)$ and $\Delta\Gamma(n)$ data from the QCM measurements with increasing annealing time t_a were done by holding the $G'_{\rm PB}$, $G''_{\rm PB}$, and $h_{\rm PB}$ parameters for the PB layer fixed at that determined from the bilayer fitting to the data collected at zero annealing time ($t_a = 0$). As described in the main text, the modulus and density of the intermix layer were taken to be the average of the PB and PS layers, $\widetilde{G}_{\rm av} = \frac{1}{2}(\widetilde{G}_{\rm PB} + G'_{\rm PS})$ and $\rho_{\rm av} = \frac{1}{2}(\rho_{\rm PB} + \rho_{\rm PS})$, leaving only a single fitting parameter: the thickness W_G of the intermix layer. The choice of $\widetilde{G}_{\rm av}$ as the arithmetic average of the PB and PS moduli was selected as the simplest approximation. To test the sensitivity of the intermix layer thickness W_G to this choice, we varied the "average" modulus $\widetilde{G}_{\rm av}$ between 30%/70% $\widetilde{G}_{\rm PB}/G'_{\rm PS}$ and 70%/30% $\widetilde{G}_{\rm PB}/G'_{\rm PS}$, corresponding to a change in $\widetilde{G}_{\rm av}$ by ≈40% in either direction, finding that W_G was well constrained varying less than 2 nm. Attempts to also treat $\widetilde{G}_{\rm av}$ as a fit parameter or add an additional fitting parameter that might account for an asymmetry in the position of the intermix layer relative to the PS/PB interface were found to be inconclusive with this analysis procedure.

Control measurements

Rubbery polymers with very low glass transition temperatures like PB (T_g^{bulk} = –96 °C for PB) frequently come with a small molecule additive that stabilizes the polymer against degradation at elevated temperatures. However, such small molecule additives can act as plasticizers altering the polymer properties slightly. We found this to be the case for this PB (M_w = 375 kg/mol, M_w/M_n = 2.4, 36% cis 1,4; 55% trans 1,4; 9% vinyl 1,2) purchased from Scientific Polymer Products when investigating local $T_g(z)$ measurements with this polymer in our previous study, Ref. (13). To remove this small molecule additive and avoid plasticization issues, we washed the purchased PB three times by dissolving the polymer in tetrahydrofuran (THF) and precipitating it in chilled methanol, as described previously (13). With the washed PB, the local $T_g(z)$ profile in the PS domain next to the PB domain is that shown in Fig. 1 where the data are from Ref. (13).

The removal of this small molecule stabilizing agent causes the potential concern that PB could begin degrading at elevated temperatures when the PB/PS bilayer films are annealed for extended lengths of time at 120 °C as the PB is then more than 200 °C above its bulk T_g. Annealing of the PB/PS bilayer films at 120 °C are done under vacuum to limit oxygen exposure when at high temperature, which should help mitigate these effects. Control measurements were performed to ensure that the measured changes in the PB/PS bilayers observed when annealing at 120 °C are not caused by changes in the PB layer due to high temperature exposure.

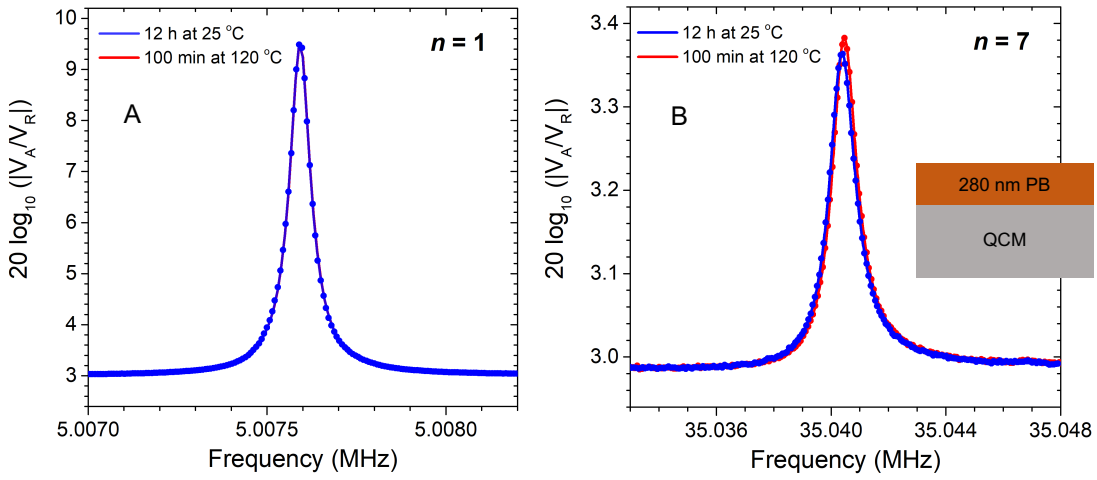

Fig. S1: Comparison of resonance frequency traces at the (A) $n = 1$ (5 MHz) and (B) $n = 7$ (35 MHz) harmonics for a single layer PB film atop the QCM sensor collected after only being held at 25 °C for 12 h (blue traces) and after annealing at 120 °C for 100 min (red traces). Little to no change is observed in $\Delta f(n)$ and $\Delta\Gamma(n)$ upon annealing at 120 °C over 100 min for a single layer PB film demonstrating no appreciable change in the PB's film thickness or viscoelastic properties with annealing time t_a.

Figure S1 shows the resonance traces of a single layer PB film with thickness of 280 nm on a QCM sensor undergoing the same annealing protocol at 120 °C as is done for the PB/PS bilayer samples. The figure compares the resonances traces at the $n = 1$ and $n = 7$ harmonics collected prior to (blue) and after (red) annealing the sample at 120 °C for 100 min. In contrast to the large changes in $\Delta\Gamma$ observed at the $n = 7$ harmonic for the PB/PS bilayers, as was shown in Fig. 2, there is no appreciable shift in the resonance frequency or dissipation between the pre-annealed data and that collected after 100 min of annealing at 120 °C. This demonstrates that there is no meaningful change in either the film thickness or viscoelastic properties of the PB films within this annealing range. For annealing times in significant excess of 100 min ($t_a \geq 200$ min), we did observe a progressive decrease in the $\Delta\Gamma(n = 7)$ data that could potentially be associated with degradation of the PB layer when annealed for extended periods at such high temperatures above its T_g. This is one of the factors that contributed to our decision to limit the annealing time at 120 °C to 100 min.

Figure S2 further compares the evolution of the dissipation shift $\Delta\Gamma$ at the $n = 7$ harmonic with annealing time t_a at 120 °C for a series of different control samples. Data for three different single layer PB films are shown (open triangles) demonstrating that the dissipation shift $\Delta\Gamma_{n=7}(t_a)$ is constant to within 10% with annealing at 120 °C for 100 min. (The gray data were shifted slightly to account for small differences in the initial value of $\Delta\Gamma_{n=7}(t_a)$ at $t_a = 0$ from sample to sample.) In contrast, data for a PB/PS bilayer sample (solid squares) demonstrates the significant ≈50% decrease in $\Delta\Gamma_{n=7}(t_a)$ with annealing at 120 °C that occurs over the 100 min. Data are also shown for a control sample corresponding to a PS/PS bilayer

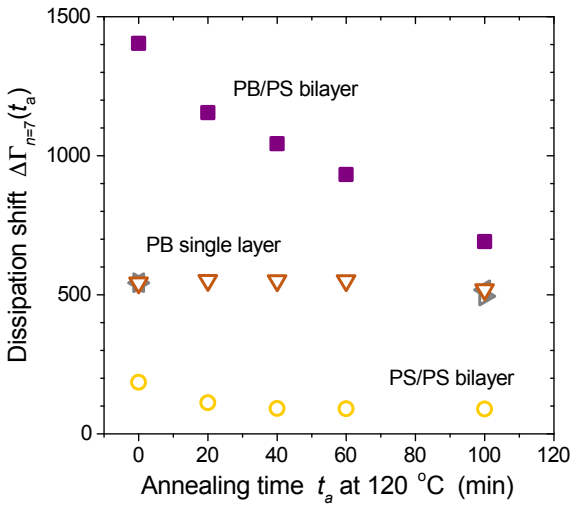

Fig. S2: Values of the dissipation shift at the 7th harmonic $\Delta\Gamma_{n=7}(t_a)$ as a function of cumulative annealing time t_a at 120 °C. The PB/PS bilayer data (solid squares) demonstrate a pronounced decrease in dissipation with annealing time. In contrast, three different single layer PB samples (open triangles) illustrate that PB is stable to within 10% during 100 min of annealing at 120 °C. A control sample of a PS/PS bilayer film is also shown (open circles) for comparison.

sample (open circles) showing an initial decrease in $\Delta\Gamma_{n=7}(t_a)$ with annealing time at 120 °C associated with the intermixing of the two PS/PS layers to form a single continuous medium.

References

1. J. Genzer, R. J. Composto, The interface between immiscible polymers studied by low-energy forward recoil spectrometry and neutron reflectivity. *Polymer* **40**, 4223–4228 (1999).
2. R. A. L. Jones, R. W. Richards, *Polymers at Surfaces and Interfaces*. (Cambridge University Press, Cambridge, UK), (1999).
3. J. A. Forrest, K. Dalnoki-Veress, Sub-glass-transition temperature interface formation between an immiscible glass rubber pair. *Journal of Polymer Science Part B: Polymer Physics* **39**, 2664–2670 (2001).
4. D. Rigby, J. L. Lin, R. J. Roe, Compatibilizing effect of random or block copolymer added to binary mixture of homopolymers. *Macromolecules* **18**, 2269–2273 (1985).
5. E. J. Kramer, Depth profiling methods that provide information complementary to neutron reflectivity. *Physica B: Condensed Matter* **173**, 189–198 (1991).
6. R. R. Baglay, C. B. Roth, Local glass transition temperature Tg(z) of polystyrene next to different polymers: Hard vs. soft confinement. *Journal of Chemical Physics* **146**, 203307 (2017).
7. C. D. Han, S. B. Chun, S. F. Hahn, S. Q. Harper, P. J. Savickas, D. M. Meunier, L. Li, T. Yalcin, Phase Behavior of Polystyrene/Polybutadiene and Polystyrene/Hydrogenated Polybutadiene Mixtures: Effect of the Microstructure of Polybutadiene. *Macromolecules* **31**, 394–402 (1998).
8. R.-J. Roe, W.-C. Zin, Determination of the Polymer-Polymer Interaction Parameter for the Polystyrene-Polybutadiene Pair. *Macromolecules* **13**, 1221–1228 (1980).
9. Y. J. Gagnon, J. C. Burton, C. B. Roth, Physically intuitive continuum mechanics model for quartz crystal microbalance: Viscoelasticity of rubbery polymers at MHz frequencies. *Journal of Polymer Science* **60**, 244–257 (2022).
10. J. Brandrup, E. H. Immergut, E. A. Grulke, A. Abe, D. H. Bloch, eds., *Polymer Handbook*. (Wiley, New York), 4th edition, (1999).
11. R. H. Colby, L. J. Fetters, W. W. Graessley, The melt viscosity-molecular weight relationship for linear polymers. *Macromolecules* **20**, 2226–2237 (1987).
12. D. Johannsmann, *The Quartz Crystal Microbalance in Soft Matter Research: Fundamentals and Modeling*. (Springer International Publishing, Switzerland), (2015).
13. B. L. Kasavan, R. R. Baglay, C. B. Roth, Local Glass Transition Temperature Tg(z) Profile in Polystyrene next to Polybutadiene with and without Plasticization Effects. *Macromolecular Chemistry And Physics* **219**, 1700328 (2018).